FPRINT-92-14

Fermilab Library
0 1160 0010625 4

19

Predictability of Charmonium Levels From a Range of Good Fits

Eric Altshuler and Dennis Silverman
Department of Physics, University of California, Irvine, Irvine, CA 92717

A QCD motivated potential with five parameters and a cutoff on high virtual momentum is used in a relativistic bound state equation to examine the predictability of such models by comparing with the seven well established charmonium levels. The predictions of potential models are really ranges for new levels given by the ranges of parameters that give good fits, rather than the single best fit. The best test of the models are done using parametrizations which are physically expected from QCD. The range of parameters that give good fits is presented in three dimensional plots by surfaces at fixed standard deviations from the known levels. Predictions for new levels in terms of splittings from related levels are shown across these surfaces by color or shading. We also show the minimum deviation analog of maximum likelihood plots with two different level splittings for axes. These show the best fits for each pair of values for the predictions and any correlations between them. For the ${}^1P_1 - {}^3P_{\rm cog}$ splitting we find the predictions not to be sharp but to cover a range of several MeV both positive and negative with $V_0 = 0.3$ GeV closest to experiment. The correlation with the $\psi' - \eta_c'$ splitting prediction is weak, and values for this splitting center around 40 MeV with a range of order 20 - 60 MeV. To range as high as the single experimental observation of 92 MeV, such a poor fit to the seven levels is needed that the model lacks any significant predictability.

U. C. Irvine Technical Report 92-35

1992

I. INTRODUCTION

The predictability of a potential model with parameters is only in a very limited sense given by the predictions with the best fit parameters. At the least one would like to give error bars to the prediction, which should arise by considering all "good" fits with the corresponding range of parameters, and the range of predictions given by this range of parameters. In actual fact the shape in parameter space of a surface of constant standard deviation is not a simple oval about the best fit, but a more complicated surface, which is convex in some dimensions and approaches an asymptotically constant shape in other variables. In this paper we begin by showing such a contour shape in four variables of a six parameter fit. We then can make predictions which are weighted by the goodness of the fit. These can be shown in a histogram for each splitting separately. We can also show the analog of maximum likelihood plots and contours show the correlations among two output splittings predictions. These could be useful in using the information when one splitting is found to put further limits on an unknown splitting. In this paper we apply this to the charmonium spectrum and show the range of predictions for the ${}^1P_1 - {}^3P_{\rm cog}$ splitting, the $\psi' - \eta_c$ splitting, and for the ${}^3D_2$ and ${}^1D_2$ levels the splitting from the ψ' or ${}^3D_1$ level, i. e. ${}^3D_2 - {}^3D_1$, and also the ${}^3D_2 - {}^1D_1$ splitting. The D_2 levels are supposed to have narrow widths due to having the wrong quantum numbers for decay into $D - \bar{D}$ states.

We use a relativistic bound state equation[1, 2] which has a four component wave function, reduces in the non-relativistic limit to the Schrodinger equation with Fermi-Breit spin-orbit and spin-spin couplings, and reduces to the Dirac equation in the limit of a heavy fermion with a light fermion. The vector and scalar interactions are separated with the gauge invariant vector containing asymptotically free gluon exchange and the scalar containing a linear potential. In this paper we modify the previously considered interactions[1] by including a parameter c_0 in $\alpha_s(q^2) = (12\pi/27)/ln(c_0 - q^2/\Lambda_R^2)$ and a constant V_0 in the linear scalar potential $V_S = \kappa r + V_0$. The bound state equation was previously applied with good agreement to the radiative transitions of charmonium and b-quarkonium[3], to f_B, and to the W-exchange contribution to the D_0 lifetime[5].

We demonstrate ways to visualize predictions in the space of the parameters of the potentials using isosurfaces of equally good overall fits. The values of a given prediction can be displayed by different values of gray scale or by different colors on these surfaces. We also demonstrate the minimum deviation or best fit method (the analog of the maximum likelihood method) for finding the minimum standard deviation for a single value of a prediction or for a pair of predictions. The latter is shown in correlation plots. We find that the predictions for the ${}^1P_1 - {}^3P_{\rm cog}$ range from -4 MeV to +3 MeV when $V_0 = 0.3$ GeV in a good fit region. We also find

that the single experimental observation for the $\psi' - \eta_c'$ splitting of 92 MeV can be accounted for at the edge of a poor fit region that allows any value from 5 MeV to 90 MeV and in which the model then lacks predictability..

The errors or range of standard deviation of the fits for a given theoretical model is analogous to the statistical error associated with an experiment. The standard deviation improves as more levels (data) are fit, restricting the range of good parameters and the range of predictions. This improvement is illustrated in the correlation plots where knowledge of one new level restricts the range of another. The differences between different theories which include different effects is then more analogous to the systematic error. Researchers often take the less well defined differences between models as the range of predictions, while here we try to illustrate that each model also has its own intrinsic statistical range of uncertainty as well. Comparisons of these between different models may well show overlaps of their statistical ranges. We use as many parameters as possible here in order to simulate a whole range of models.

In section 2 we describe the potential and the spectra we fit to. In section 3 we describe the six parameters and show how we treat them to analyze all six of them together. In section 4 we show the multidimensional plots for good fit iso-surfaces in the parameter space. In section 5 we show the minimum deviation method for showing the range of predicted splittings and correlations between predictions. Section 6 summarizes the use and value of these methods.

II. RELATIVISTIC INTERACTIONS, PARAMETERS, AND SPECTRA

We refer the reader to Ref. 1 for the formulation of the relativistic integral equation being used for charmonium. Here we only describe the modified interactions which include additional parameters. For the asymptotically free gluon exchange treated as a vector interaction coupling to γ_μ quark currents we use the form

$$V_V(q^2) = (4/3)4\pi\alpha_s(q^2)/q^2, \tag{1}$$

$$\alpha_s(q^2) = (12\pi/27)/ln(c_0 - q^2/\Lambda_R^2), \tag{2}$$

where $q^2 = q_0^2 - \vec{q}^2$. The new parameter is c_0 which is kept greater than one so that the q^2 cuts are only in a physically correct region, and also since $c_0 = 1$ would result in the Richardson potential which has a Fourier transform which is linear in r. The linear potential must not occur solely in a vector interaction in a relativistic equation since it produces a Klein paradox with the lower Dirac components seeing a linearly falling potential. Recent studies of QCD also show that the linear potential is scalar. In the plots, α_s at $q^2 = 0$ will be shown instead of c_0, since its strength is more directly related to effects on the spectra, and since it is dependent only on c_0 and not Λ_R

$$\alpha_0 = \alpha_s(0) = (12\pi/27)/ln(c_0). \tag{3}$$

For the scalar interaction we use

$$V_S(r) = \kappa r + V_0 \tag{4}$$

where V_0 represents the gluon field surrounding the quarks in addition to the linear part from the length of the string.

In order to get very accurate predictions we use only the seven well established levels of charmonium, namely $J/\psi(3097)$, $\psi(3685)$, $\psi(3770)$, $\eta_c(2980)$, $\chi_{c0}(3415)$, $\chi_{c1}(3510)$, and $\chi_{c2}(3555)$. The η_c' has not been confirmed, and its location is far from our and other potential model calculations. The $\psi(4040)$ and $\psi(4160)$ are not unambiguously seen, and it is not easy to identify $\psi(4160)$ as the $2D$ state since it should have a small coupling to e^+e^- (see the minireview in Review of Particle Properties[7], 1986). In any case, these two levels, along with the $\psi(4415)$, are expected to be heavily shifted and broadened by coupling with the $D - \bar{D}$ set of channels above threshold. Thus we constrain our search for good fits to the seven established levels listed above.

III. PARAMETERS AND THEIR RANGES

While we formally evaluate results for 6 parameters, to do it in finite computing time we take advantage of understanding the physical dependence on them. For the charm quark mass, m_c, we note that the spin-orbit and spin-spin splittings depend as m_c^{-2}, but the shift in m_c over the good fits is at most 300 MeV. The splittings thus vary slowly with m_c, but the overall levels shift together rapidly since the basic energy is $2m_c$. The mass m_c is adjusted for each set of parameters to minimize the standard deviation of the calculated values of the seven levels from their experimental values. The final m_c is then an output function of the other parameters. This eliminates displaying the obvious variation in predictions with this parameter.

In varying the zero point of the linear potential, we take only a few values of V_0. Since the scalar V_0 adds to $2m_c$ to give the base meson mass for the spectra, a positive V_0 gives a lower m_c. To start each set of parameters then the J/ψ is calculated first from an initial m_c^0, and a δm_c^0 is found which is necessary to be added to give the J/ψ at its correct value. This is iterated again until no significant shift occurs. The effect is that the dynamical quark mass in the potential and splittings varies over the parameter ranges and enhances or decreases the splittings. This produces a δm_c^0 with a range of at most -300 to +300 MeV from the starting $m_c^0 = 1.58$ GeV $- V_0/2$ over our wide range of parameters.

The standard deviation used for $N = 7$ levels is then formed from calculated levels E_c^i and experimental levels E_e^i by

$$\sigma = \sqrt{\sum_{i=1}^{N}(E_c^i + 2\delta m_c - E_e^i)^2/(N-1)}. \tag{5}$$

δm_c is chosen to minimize σ giving

$$0 = \sum_{i=1}^{N}(E_c^i + 2\delta m_c - E_e^i) \tag{6}$$

$$\delta m_c = 1/(2N)\sum_{i=1}^{N}(E_e^i - E_c^i) \tag{7}$$

Eqn. (6) is equivalent to moving the center of mass of the calculated levels to that of the experimental seven levels. Using this δm_c in Eqn. (5), the value of σ for each set of parameters is output. The final m_c is given by

$$m_c = m_c^0 + \delta m_c^0 + \delta m_c \tag{8}$$

The relativistic equation which is an extension of the Dirac equation requires a cutoff at high virtual three-momentum[1] p, and we take the strong form which has been needed for some calculations[5]

$$S(p) = 1/(1 + p^2/\Lambda_c)^2 \tag{9}$$

making Λ_c the third parameter.

The parameter controlling the falloff of the vector coupling strength with q^2 is Λ_R^2. We observe in Eqn. (2) that as Λ_R approaches infinity, the coupling strength approaches a constant, namely, α_0 in Eqn. (3). Thus the surfaces of constant standard deviation approach a shape which does not vary with Λ_R as it increases indefinitely. In practice, we find that beyond $\Lambda_R = 1$ GeV, there is little variation, and we use this as the upper limit for Λ_R in the displays.

In order to present minimum deviation plots, which are the analog of maximum likelihood plots, and include contours up to $\sigma = 20$ MeV, we should include all parameters that yield such a σ or less. However, the shape in the parameter space (see figures below) is not a contained ovular shape. Extremely small Λ_R will cut down the effective α_s, and can be compensated for by large Λ_c, increasing the virtual momentum phase space, or by larger κ, confining more. However, very large Λ_c will make the wave function at the origin and thus the e^+e^- decay width unacceptably large, and κ cannot be too large from Regge trajectory slopes. So we limit the κ and Λ_c parameters, but over a still very large range. The lowest standard deviation we get is about 9 MeV for $V_0 = 0.3$ GeV, and the "good fit" range about that is not quantifiable in terms of a confidence level, but as a matter of experience in making predictions and in the accuracy level needed for the specific predictions.

IV. ISO-SURFACES OF STANDARD DEVIATION FOR THE CHARMONIUM LEVELS

Taking only certain values for V_0 we proceed to display three dimensional sections of the standard deviation surfaces in the four variable space of Λ_R, κ, Λ_c and α_0. With the above seven spectral levels and computing strategy, we found the best standard deviation was about 9 MeV for $V_0 = 0.3$ GeV. Since most of the splittings are on the order of 100 MeV, in order to work to 20% accuracy we display the surfaces of standard deviation of 20 MeV or 25 MeV to make effects in the isosurfaces clearer.

To begin, we demonstrate the relative constancy of the shape for Λ_R approaching 1 GeV. In Fig. 1 is plotted the standard deviation surface of $\sigma = 20$ MeV, using the axes Λ_c, Λ_R, and α_0 for fixed $\kappa = 0.157$ GeV^2 and $V_0 = 0.3$ GeV. The ranges of the parameters for which the calculations were made and plotted are: $\Lambda_c = 1.5$ to 12.0 GeV, $\Lambda_R = 0.07$ to 1.0 GeV, $\alpha_0 = 0.1$ to 1.3, and $\kappa = 0.05$ to 0.30 GeV^2. In each parameter the calculations were carried out for 15 values uniformly spaced in the range. We note the effect in Eq. (2) that as $\Lambda_R \to \infty$, the strength α_s does not decrease with increasing $|q^2|$. Thus at large Λ_R the shape becomes asymptotic or independent of Λ_R. In this limit then, smaller α_0 is needed to give the same binding effect as seen in the constant standard deviation surface in Fig. 1. Conversely, as Λ_R gets small, the logarithmic cutoff occurs rapidly, and larger α_0 is needed.

We also show in Fig. 1 by the grayness on the surface the value of one of the predicted splittings. In this case we show the ${}^1P_1 - {}^3P_{\rm cog}$ splitting as white when it is in the range of 0 to 2 MeV, and as dark gray elsewhere. This covers the range containing the experimental result[8] of E760 and occurs for most Λ_R but only for the larger $\alpha_0 > 0.3$ with larger α_0 at smaller Λ_R required.

The Λ_c cutoff acts in the integral over the virtual three momentum p' of the momentum space integral equation[1] for the wavefunction $\psi(p)$ at momentum p. This effectively limits $q^2 = (p - p')^2 < O(4\Lambda_c^2)$. Thus this acts as a short distance cutoff to the coulombic-like QCD potential, effective at $r_c \approx 1/\Lambda_c$. The $S(p, \Lambda_c)$ cutoff represents the physical effects of multiquark or two-meson channels removing probability from the $q - \bar{q}$ channel in the integral equation. At small Λ_c, the effective strength is reduced by a lack of phase space, and is made up by an increase of α_0 strength for the good fits.

The effect of lighter m_c for V_0 positive is to give larger spin-orbit and spin-spin splittings, which depend on the short distance vector potential, and this is balanced by restricting the phase space with smaller Λ_c, thus disallowing shorter distances in the potential in the good solutions.

Next, for fixed $\Lambda_R = 0.43$ GeV we show in Fig. 2 the 25 MeV standard deviation surface with axes Λ_c, κ, and α_0, as shown. We see that larger κ in the positive linear

κr potential is balanced again by increased α_0 attraction. By shading we indicate in this figure the regions producing various values of the $\psi' - \eta_c'$ splitting. The light region is for a splitting above 50 MeV, the medium gray region for splittings between 30 and 50 MeV, and the black region for below 30 MeV.

Extending the ranges of parameters further is not necessary. Either the parameter has already become asymptotic in the iso-surface shape, or it goes well beyond limits imposed from other considerations.

V. RANGES AND CORRELATIONS OF PREDICTED SPLITTINGS FOR MINIMUM STANDARD DEVIATIONS

In describing the range of predictions for a given splitting, we consider separately each possible value of the splitting, and search over the entire parameter set for the minimum value of standard deviation associated with that predicted value of the splitting. This can then be plotted as a histogram over a given range of the splitting. Since each point in the parameter space is considered equally possible, this is the appropriate method. For making predictions of two splittings simultaneously, and looking for their correlations, we search through the parameter range and find the minimum standard deviation for each given choice of the two predicted splittings, and show the result with contours at fixed values of the minimum deviations, with the predicted splittings as the axes.

We first consider the levels or splittings being searched for in Fermilab E760 in proton anti-proton annihilation. The best values are shown in Fig. 3a for $V_0 = 0.3$ GeV. On the y-axis is the splitting $\psi'(3686) - \eta_c'$ from 0 to 100 MeV, and on the x-axis is ${}^1P_1 - {}^3P_{\rm cog}$ from -15 to $+15$ MeV. The contours are at minimum deviations of 10, 15 and 20 MeV. The calculations over the parameter ranges of the potential were carried out by taking 15 uniformly spaced values in each range. The contours in this "best fit" plot are smoothed over 10 bins in each of the axis variables. The contours for $V_0 = 0$ are shown in Fig. 3b and the central contours are seen to be moved to about 3 MeV lower in the ${}^1P_1 - {}^3P_{\rm cog}$ splitting.

For $V_0 = 0.3$ GeV, Fig. 3a, we see that predictions of $\psi' - \eta_c'$ peak around 40 MeV at the $\sigma = 10$ MeV contour, and range from 20 to 60 MeV at the $\sigma = 15$ MeV contour. The contour $\sigma = 23$ MeV is needed (by extrapolation) for $V_0 = 0$, Fig. 3b, or for $V_0 = 0.3$ GeV, to reach the splitting of 92 MeV in the only observation[6, 7] of the η_c'. At this contour, the model lacks predictability as the whole range from about 5 MeV to 90 MeV is included. Comparing Figs. 3a and 3b shows that the $\psi' - \eta_c'$ splitting predictions are fairly independent of V_0.

The range of the ${}^1P_1 - {}^3P_{\rm cog}$ splitting for $V_0 = 0.3$ GeV in Fig. 3a is centered around zero at $\sigma = 10$ MeV and -4 to $+6$ MeV at $\sigma = 15$ MeV. For $V_0 = 0$ the

$\sigma = 10$ MeV contour ranges from -5 MeV to $+1$ MeV.

The new observation of the $^1P_1$ in Fermilab E760[8] giving the $^1P_1 - {}^3P_{\rm cog}$ splitting at $+1$ MeV weighs in favor of $V_0 = 0.3$ GeV and indicates that these contours may be useful near the 10 MeV contours.

These ranges may also be useful to experimenters to estimate what interval must be considered in which to evaluate the statistical significance of any peak found within this range. The presence of the $^1P_1 - {}^3P_{\rm cog}$ splitting in our calculations is due to the fact that we do not use a pure 1/r coulombic gluon potential, but have the extra asymptotic freedom logarithmic q^2 dependence built in (Eqn. (2)). At large Λ_R where the q^2 dependence decreases, we notice that this splitting also decreases, as in the white region of small positive splitting in Fig. 1.

While the $\psi' - \eta_c'$ is a spin-spin splitting, and the $^1P_1 - {}^3P_{cog}$ is a tensor splitting, their magnitudes both depend on the value of the short distance potential, and may be expected to show some correlation, as they do in Fig. 3b, but do not significantly in Fig. 3a. What is correlated is the increases of the range of the splittings in each output for an increase in standard deviation.

The $^3D_2 - {}^3D_1$ splitting is shown on the y-axis versus the $^1P_1 - {}^3P_{\rm cog}$ splitting on the x-axis in Figs. 4a and 4b for $V_0 = 0.3$ GeV, and $V_0 = -0.3$ GeV, respectively. The smoothing is over 16 bins on the y-axis and 10 on the x-axis. Little correlation is seen between the two splittings for $V_0 = 0.3$ GeV, but some occurs for $V_0 = -0.3$ GeV. The range of the $^3D_2 - {}^3D_1$ splitting in Fig. 4a is seen to be $+10$ to $+40$ MeV for the $\sigma = 15$ MeV contours centered around 25 MeV at the $\sigma = 10$ MeV contour.

For the D wave splittings, we note that if the tensor force is small, especially for D waves as compared to P waves, then the splittings are given by spin-orbit splittings and are related. For the $^3D_2 - {}^3D_1$ and $^3D_2 - {}^1D_2$ splittings the differences in the values of $\vec{L} \cdot \vec{S}$ are 2 and -1, respectively. In Fig. 5a and 5b, with x-axis $^3D_2 - {}^3D_1$ and y-axis $^3D_2 - {}^1D_2$ the scales are such to make a spin- orbit correlation line running through zero for both with a $-45°$ slope. In the left half of the contours such a correlation is seen, but not passing through zero. Thus a positive tensor force contribution of order 20 MeV must be present in the $^3D_2 - {}^1D_2$ splitting. The $^3D_2 - {}^1D_2$ splitting centers around $+5$ MeV with a range from $+2$ to $+10$ MeV at the $\sigma = 15$ MeV contour.

VI. CONCLUSIONS

In the isosurface of fixed standard deviation in parameter space we have seen how changes in one parameter of the potential can be compensated by changes in another parameter. We have also seen by displaying predictions in gray scale across the isosurface whether a given prediction is "likely" by occuring over a large range

of parameter, or whether it occurs only for a very small range of parameters, or at the extremes of the parameter range for good fits. We can further identify what features of the potential are important in each splitting. We also have seen how the shapes become asymptotic in some parameters and unbearably large in others. Later, additional constraints can be added such as those from QCD calculations of the potential shape, and also radiative decay and annihilation rates. However, since our intent here was in making predictions for spectral levels, using them as the sole input and using their own deviation to evaluate the goodness of fit was the most consistent method.

We have also shown how to judge predictions and to find correlations in the best fit minimum deviation correlation plots. Ranges for predictions for η_c', ${}^3D_2$, ${}^1D_2$, and ${}^1P_1$ are then given.

VII. ACKNOWLEDGEMENTS

This research was supported in part by the U.S. Department of Energy under Contract No. DE-FG03-91ER40679. We would like to thank Woon-Seng Choong and Dr. Allen Schiano for their help with the graphics software. We thank Profs. Mark Mandelkern and Jonas Schultz for discussions. D. S. thanks the Aspen Center for Physics for their hospitality.

REFERENCES

[1] M. Bander, D. Silverman, B. Klima, and U. Maor, Phys. Rev. D **29**, 2038 (1984).
[2] M. Bander, D. Silverman, B. Klima, and U. Maor, Phys. Lett. **13B**, 258 (1984).
[3] F. Daghighian and D. Silverman, Phys. Rev. D **36**, 3401 (1987).
[4] D. Silverman and H. Yao, Phys. Rev. D **38**, 214 (1988).
[5] D. Silverman and H. Yao, Phys. Rev. D **36**, 3392 (1987).
[6] C. Edwards, Phys. Rev. Lett. **48**, 70 (1982).
[7] Particle Data Group, p. 225, Phys. Lett. **170B**, 1 (1986)
[8] T. A. Armstrong, et al., Fermilab Preprint (1991).

FIGURES

FIG. 1. Surface of AD = 20 MeV for $V_0 = 0.3$ GeV and for fixed $\kappa = 0.157$ GeV^2 with: Λ_c from 1.5 to 12.0 GeV; Λ_R from 0.07 to 1.0 GeV; and α_0 from 0.1 to 1.3. On the isosurface is displayed in shading the predictions for the $^1P_1 - {}^3P_{\rm cog}$ with white for 0 to 2 MeV, and gray otherwise.

FIG. 2. Surface of AD = 25 MeV for $V_0 = 0.3$ and for fixed $\Lambda_R = 0.43$ GeV with: Λ_c from 1.5 to 12.0 GeV; κ from 0.05 to 0.30 GeV^2; and α_0 from 0.1 to 1.3. The shading shows the $\psi' - \eta_c'$ splitting with light gray above 50 MeV, gray between 30 and 50 MeV, and black below 30 MeV.

FIG. 3. "Best fit" correlation plots for (a) $V_0 = 0.3$ GeV, (b) $V_0 = 0$, with x-axis $^1P_1 - {}^3P_{\rm cog}$ from -15 MeV to 15 MeV, and y-axis $\psi' - \eta_c'$ from 0 to 100 MeV, showing contours of AD = 10, 15, and 20 MeV.

FIG. 4. "Best fit" correlation plots for (a) $V_0 = 0.3$ GeV, (b) $V_0 = -0.3$ GeV, with x-axis $^1P_1 - {}^3P_{\rm cog}$ from -15 MeV to 15 MeV and y-axis $^3D_2 - {}^3D_1$ from -20 to 50 MeV showing contours of AD = 10, 15, and 20 MeV.

FIG. 5. "Best fit" correlation plots for (a) $V_0 = 0.3$ GeV, (b) $V_0 = 0$, with x-axis $^3D_2 - {}^3D_1$ from -10 to 50 MeV and y-axis $^3D_2 - {}^1D_2$ from -5 to 25 MeV showing contours of AD = 10, 15 and 20 MeV.

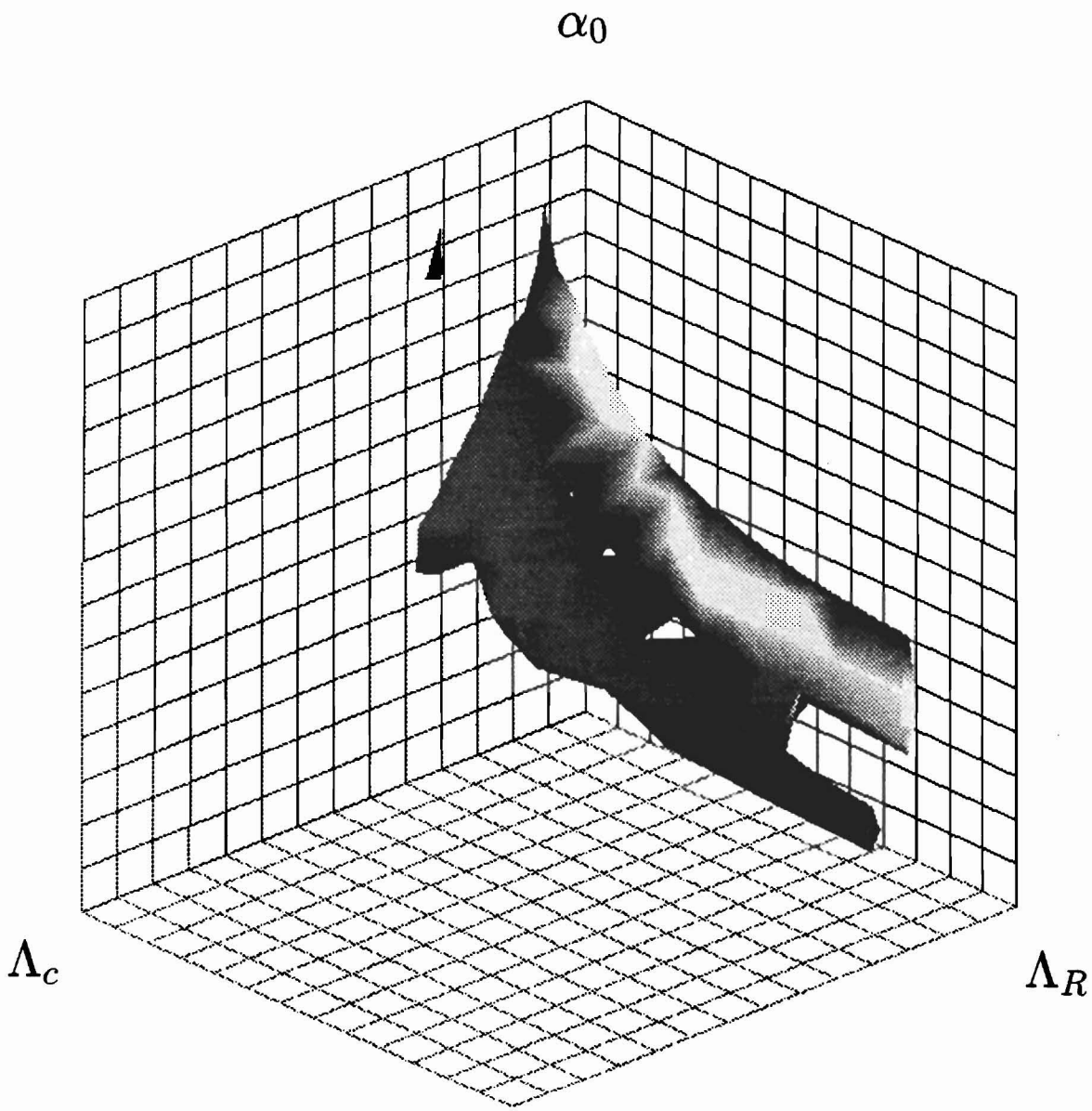

Fig. 1

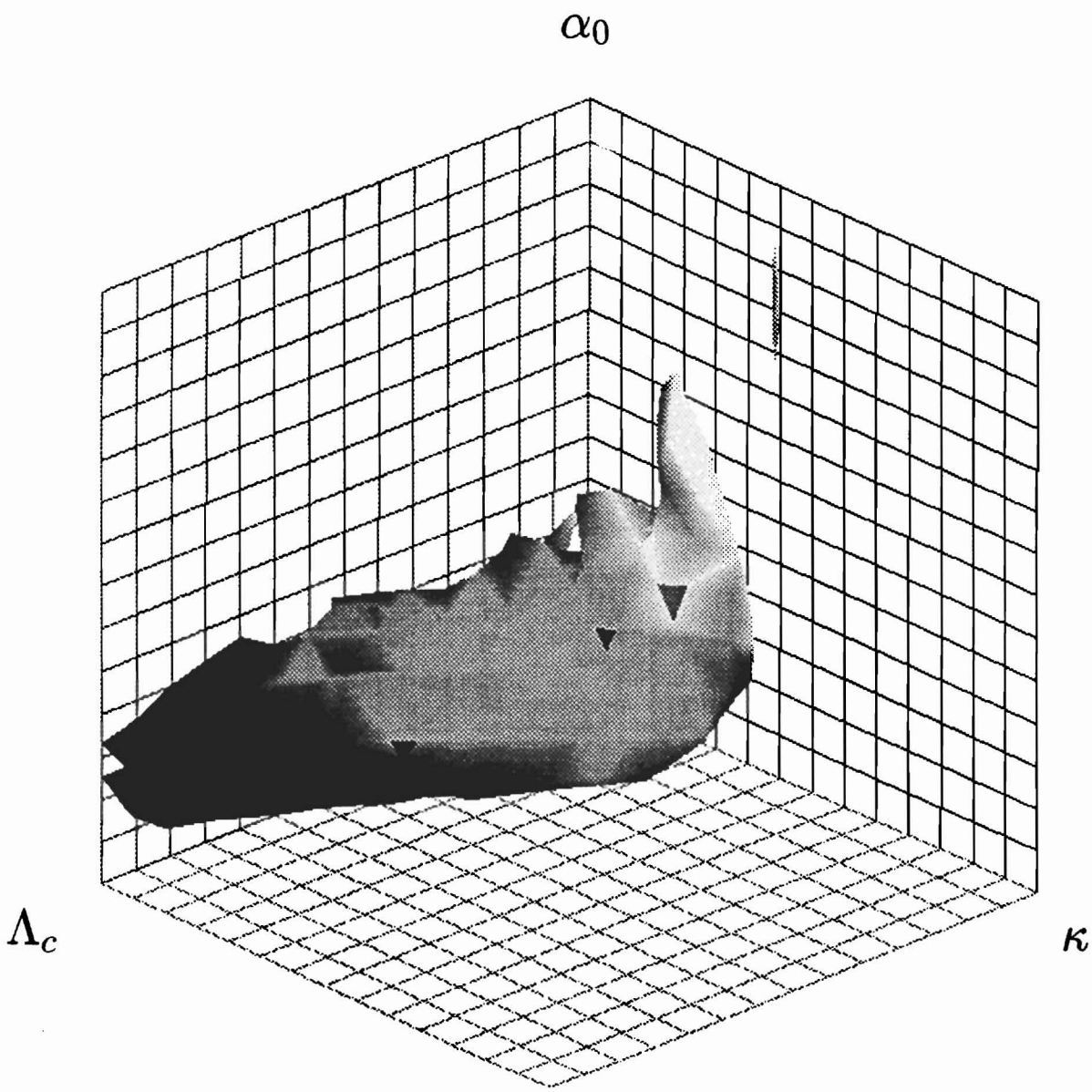

Fig. 2

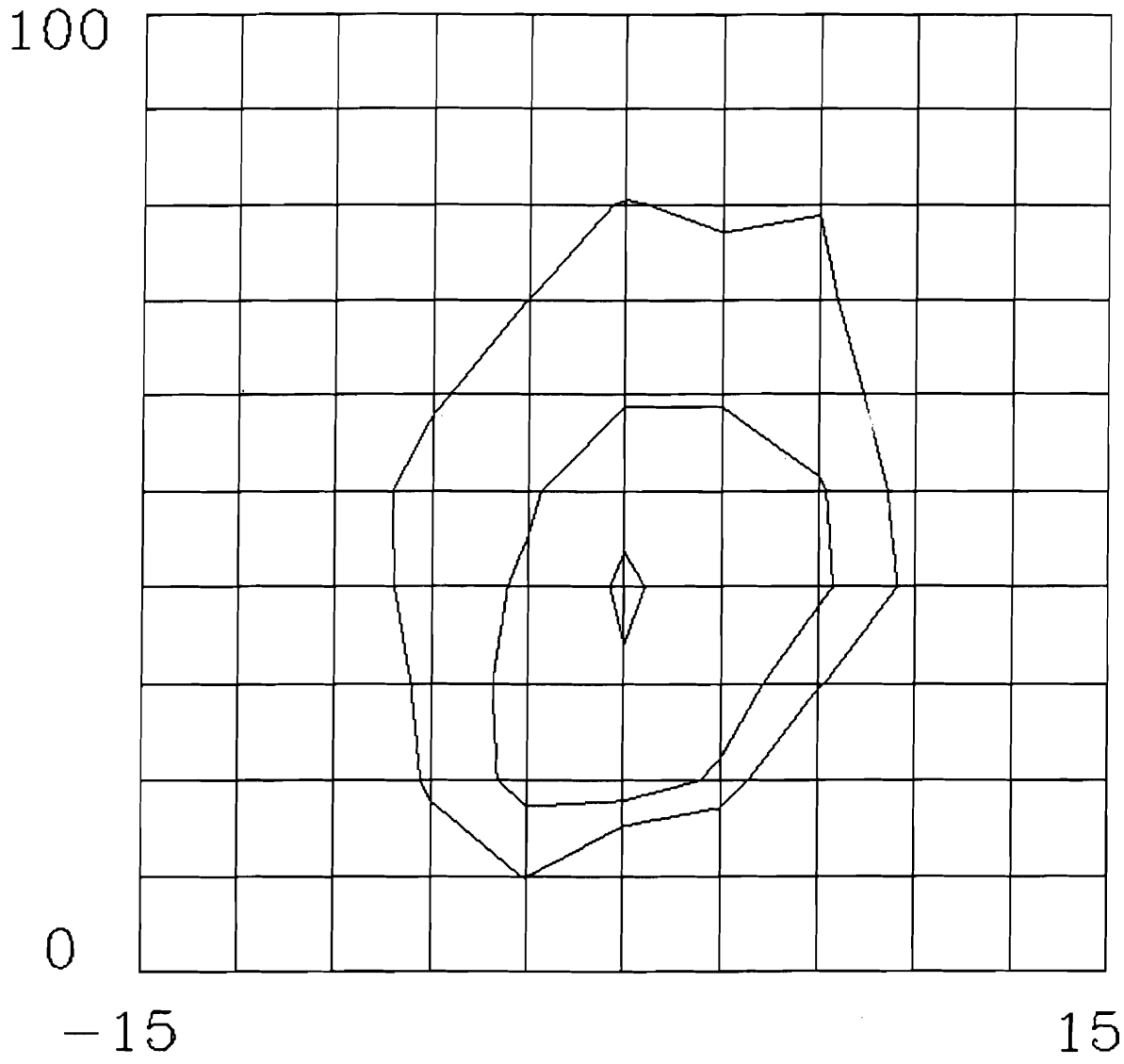

Fig. 3a

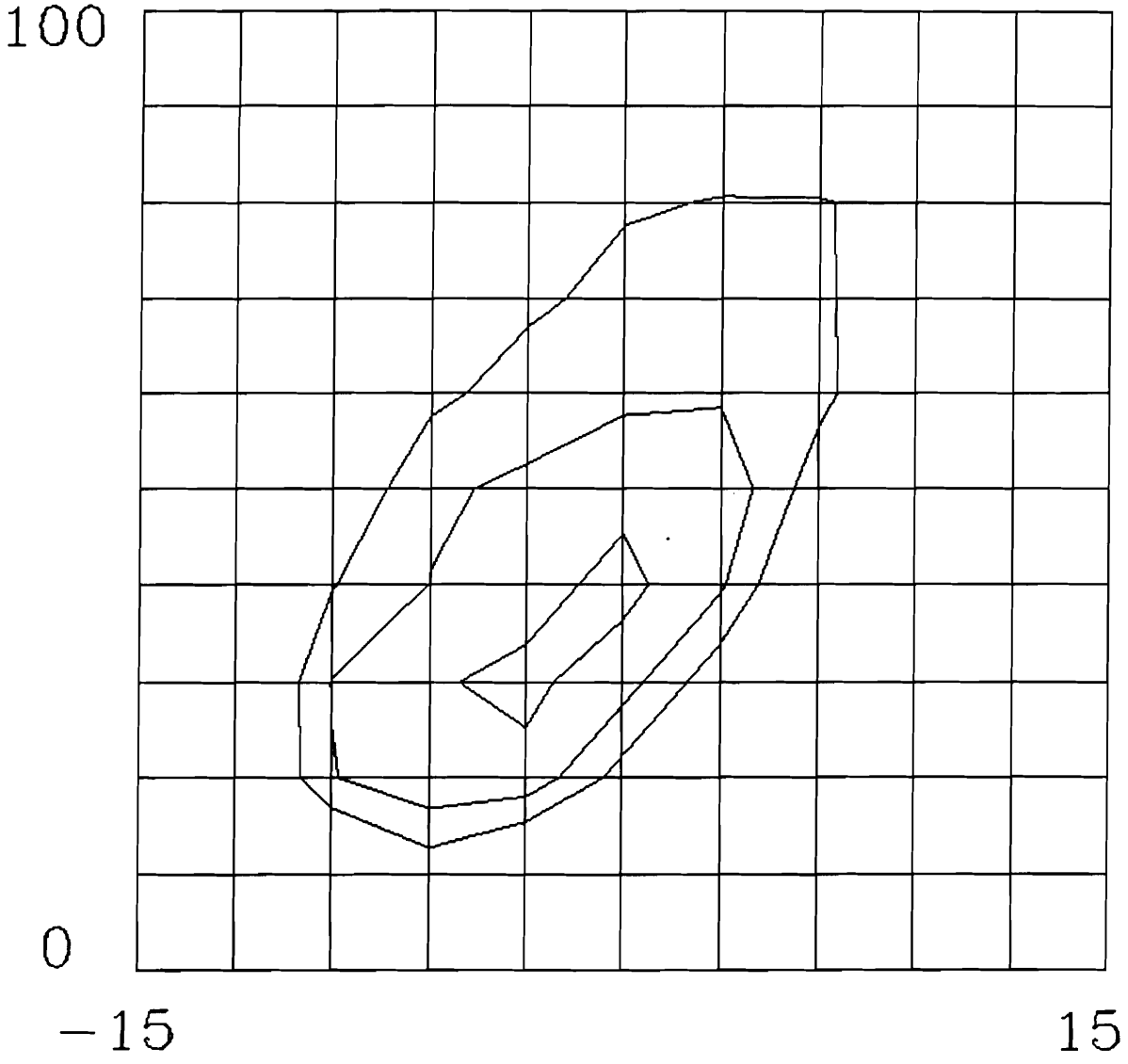

Fig. 3b

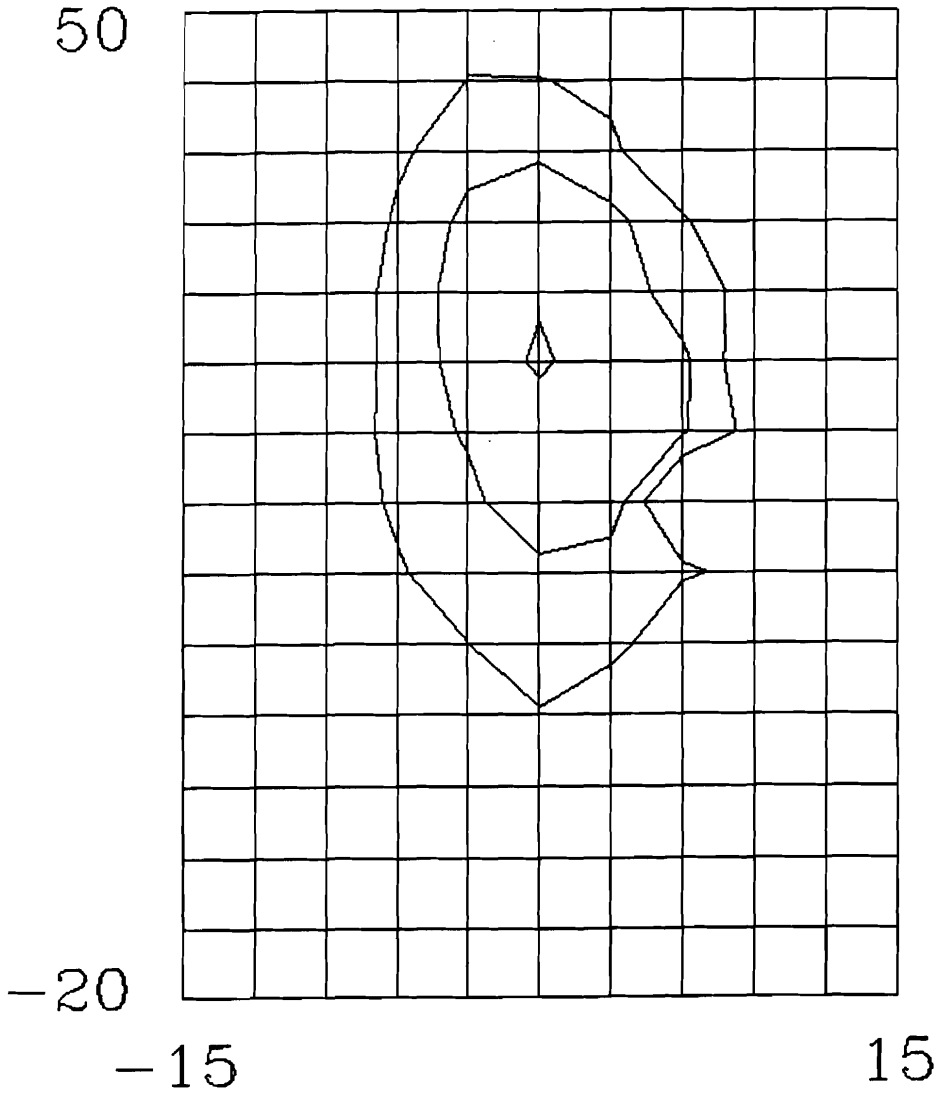

Fig. 4a

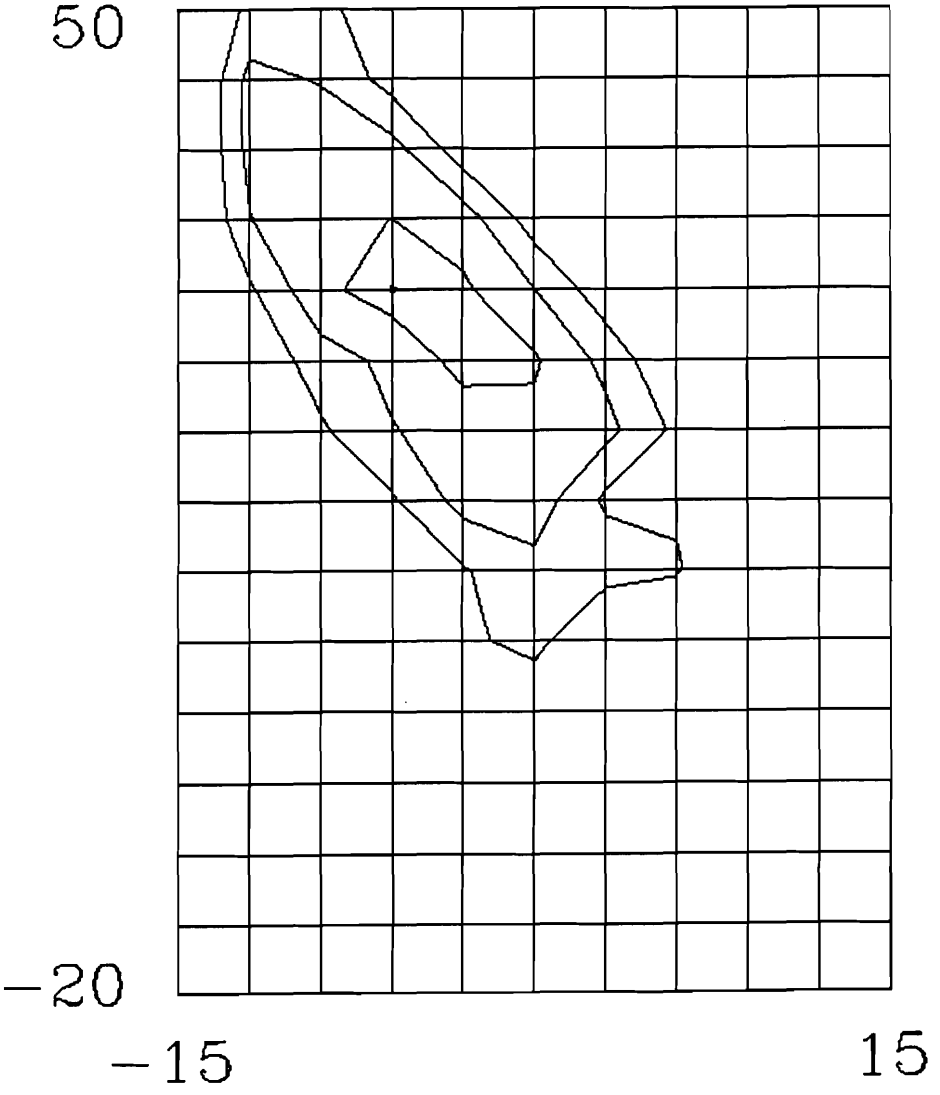

Fig. 4b

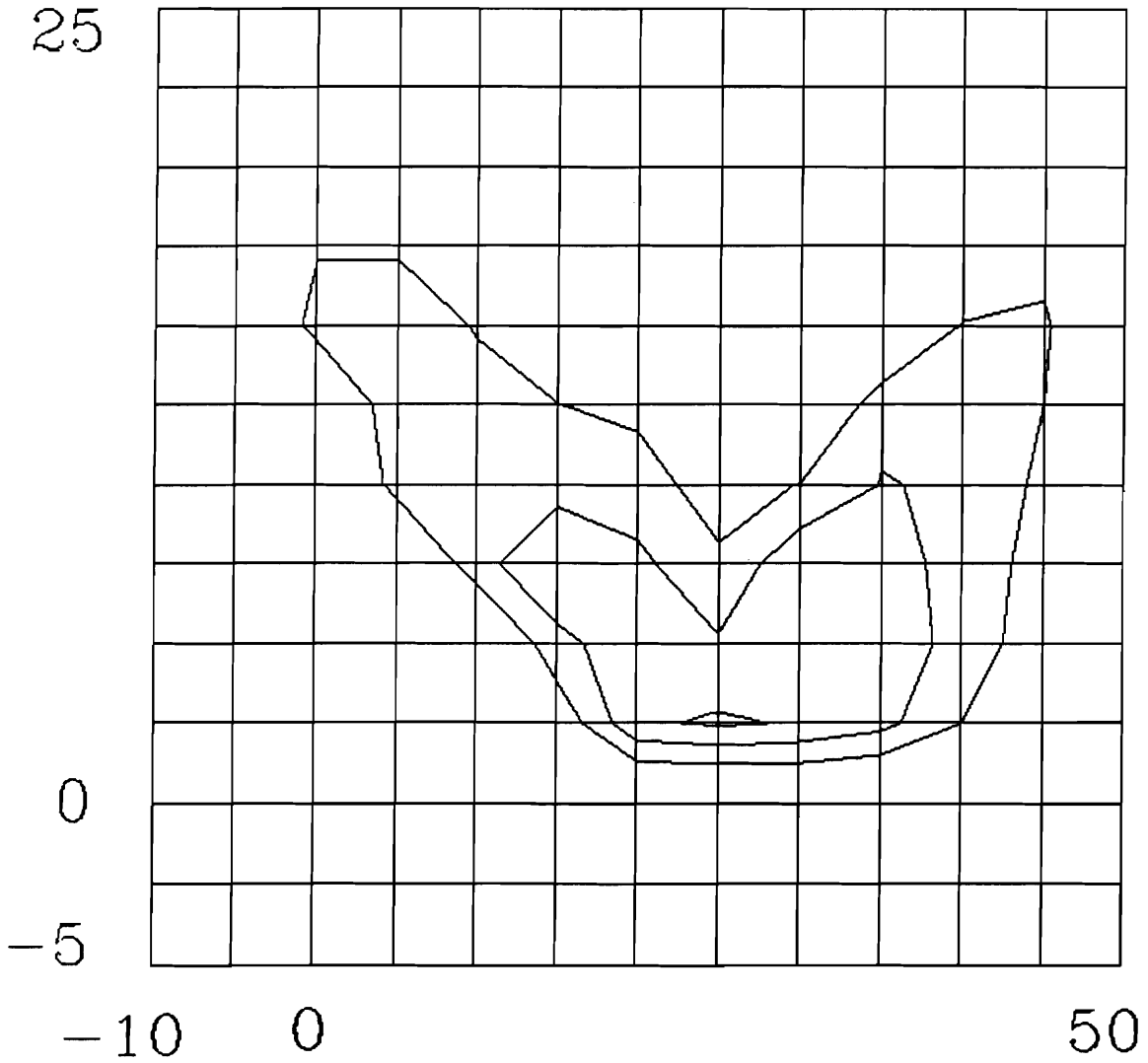

Fig. 5a

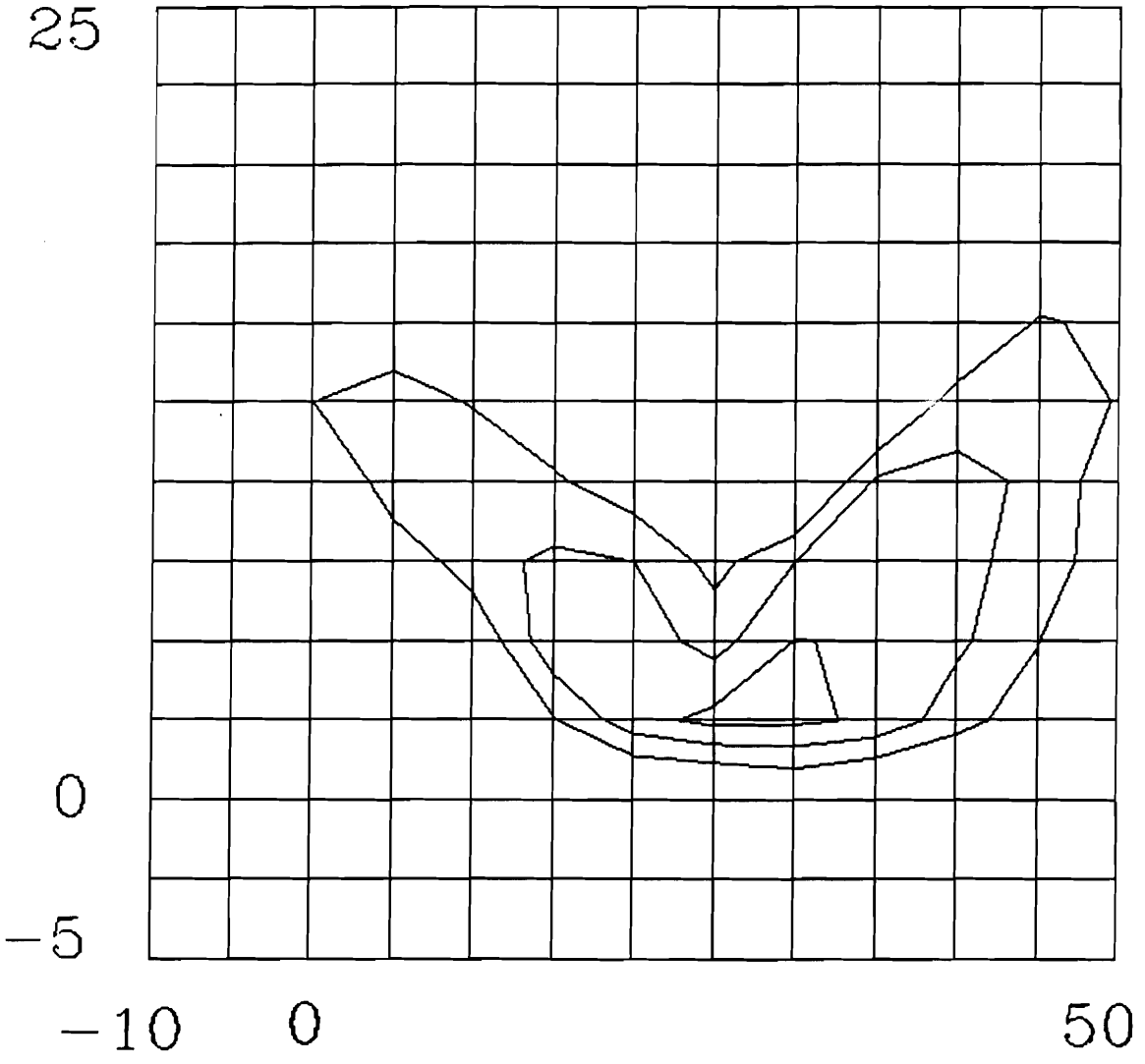

Fig. 5b